Article

Bayesian Inference of Phenomenologycal EoS of Neutron Stars with Recent Observations

Emanuel V. Chimanski[1,‡], Ronaldo V. Lobato[2,3,‡], Andre R. Goncalves[4,‡] and Carlos A. Bertulani [2,‡]

Citation: Chimanski, E. V.; Lobato, R. V.; Goncalves A. R., Bertulani, C. A. Title. *Preprints* **2021**, *1*, 0. https://doi.org/

Received:
Accepted:
Published:

1 National Nuclear Data Center, Brookhaven National Laboratory, Upton, NY, USA
2 Department of Physics and Astronomy, Texas A&M University - Commerce, TX, USA
3 Universidad de los Andes, Bogotá, Colombia
4 Lawrence Livermore National Laboratory, Livermore, CA, USA
* Correspondence: chimanski@bnl.gov, r.vieira@uniandes.edu.co, goncalves1@llnl.gov, carlos.bertulani@tamuc.edu
‡ These authors contributed equally to this work.

Abstract: The description of stellar interiors remains as a big challenge for the nuclear astrophysics community. The consolidated knowledge is restricted to density regions around the saturation of hadronic matter $\rho_0 = 2.8 \times 10^{14}$ g cm^{-3}, regimes where our nuclear models are sucessfully applied. As one moves towards higher densities and extreme conditions up to five to twenty times ρ_0, little can be said about the microphysics of such obejects. Here, we employ an MCMC strategy in order to acess the variability of polytropic three-pircewised models for neutron star equation of states. With a fixed description of the hadronic matter we explore a variety of models for the high density regimes leading to stellar masses up to 2.5 $M_\odot$. In addition, we also discuss the use of a Bayesian power regression model with heteroscedastic error. The set of EoS from LIGO was used as inputs and treated as data set for testing case.

Keywords: Bayesian Inference, MCMC, Equation of State, Heteroscedastic, Neutron Star, Astrophysics

1. Introduction

Neutron stars (NS) are supernova remnants, with a strong gravitational field and rapid rotation. They are objects with nuclear matter in one of the highest density states in the Universe. The matter in their interior is compacted to values from a few g cm^{-3} on their surface to possibly more than 10^{15} g cm^{-3} in their center. The NS have become, alongside black holes, vital sources of gravitational waves, and although they have been discovery more than 50 years as pulsars [1], its internal structure still is not thoroughly understood. Part of the challenge, relates to the extreme physical environments, e.g large matter and energy densities, and the associated limits of our current models that contain parameters adjusted to reproduce, at their best, nuclear properties on natural conditions present on Earth.

Recently, this picture has started to change with multimessenger observations [2] from binary NS mergers [3,4]. Those constraints provide the opportunity for a more detailed study about some of the parameters that describe global properties of NS such as radius constraints [5,6], tidal deformabilities [7], maximum mass [8] and other global properties. All this information, are intimately associated with the equation of state of the NS, and once one constrains the global properties, the microphysics can to be constrained as well. The GW170817 event, for example, besides the breakthrough of being the first gravitational wave detection, was also a source of many studies that considered the impact of the observation on internal aspects of the star. The impact of the NS crust on the equation of state was investigated [9], as well as the effects of an isovector–scalar meson into the quark–meson coupling description of nuclear matter [10], and also different Skyrme-like parametrizations [11]. Non-parametric inference showed that the event favors soft EoS [12]. Critical examinations of the EoS of dense matter were performed [13] considering the nuclear physics in the chiral effective field theory framework, but still left some understanding to be improved in regions of high densities of the EoS. The association with electromagnetic counterparts of the event, lead to the first time to a joint-constraint. Using the binary's

Preprints (www.preprints.org) | NOT PEER-REVIEWED | Posted: 6 May 2022 doi:10.20944/preprints202205.0073.v1

tidal deformability parameter, simulations of EM observations within numerical relativity and Kilonova models, extreme EoS models were ruled out, theoretically the stiffest and softest ones, e.g., see figure 2 of Ref. [2]. Statistical Bayesian methods were applied in the context of the GW170817 event, where microscopic models of cold neutron stars using chiral effective models [14] were studied. Recently, the GW event with X-ray sources we combined and studied with the relativistic mean field models [15]. Besides the electromagnetic counterpart of the binary merger, another important recent electromagnetic measurement was done by the NASA's *Neutron Star Interior Composition Explorer* (*NICER*) [16], also constraining the mass-radius of the pulsar PSR J0030+0451 [17,18]. While the astronomical data was gathered and studied theoretically, experiments on Earth have also been performed. For example, the Lead Radius EXperiment (PREX-2) which has provided a better understanding of the nuclear matter around the saturation density, has a direct implication for the crust of neutron stars. The extrapolation of the data to higher densities has limited the stellar radii to $13.25 \lessapprox R_{1.4} \lessapprox 14.26$ km, meaning that the EoS should have a softening in the intermediate region and a stiffening at the high densities. This, in turn, could lead to a phase transition in the stellar core. The increment in observational data, has helped to establish further constraints on the dense matter EoS opening a rich field for statistical and machine learning models [19–23].

The description of nuclear matter around the nuclear saturation density $\rho_0 = 2.8 \times 10^{14}$ g cm^{-3} $= 0.17$ fm^{-3} is well understood in terms of hadron physics. The microphysics at intermediate densities is yet far away from a consensus with a wide range of possible models. The debate includes the binding nature of NS with theories considering self-bound quarks or simply with gravity-bound systems. The asymptotic behavior of the EoS, on the other hand, has been understood in the context of quark matter [24]. As the details of the nuclear models are out of the scope of this work, we refer to Refs [25–33] and references within for more information.

In this work, we separate the description of the equation of state into a three-piece polytropic functional. We based our approach in the work by Read et al. 2009 [34] where a piecewise EoS was fitted with a direct cost function minimization. Here, we extend this picture to a larger class of models made possible with modern computing resources. We adjust the position of each piece of the EoS to better reproduce the observational data, and then perform a Bayesian Inference with Markov Chain Monte Carlo on the polytropic exponent of each case. This approach provides an assessment of the impact of variations in the EoS at intermediate and high densities on the mass radius diagram of the star.

One of our objectives is to determine the mass and radius of a selection of stars in correlation to the description of nuclear matter modeled by the EoS. In this way, we can systematically use different EoS parameterizations to determine relevant characteristics of neutron stars. In addition to that, we discuss the use of a Bayesian statistical model with heteroscedastic errors. This enables the training of statistical models based on EoS generated by different nuclear physics pictures. Due to the various parameterizations present in the microscopic models, the result set of all equation of states has a variance that increases alongside density (heteroscedasticity). This behavior can be captured by models with scattering residuals at different levels of the EoS when trained simultaneously with the NumPyro probabilistic programming library[1]. Here we use the set of EoS from LIGO as input and handling the data set as a test case.

2. The structure of Neutron Stars

The description of NS comprises both the quantum mechanical and general relativity worlds. The properties of particles that constitute the stellar matter are considered via equation of state obtained from quantum mechanics in flat space. The EoS is present in the energy-momentum tensor $T^{\mu\nu}(\rho, P(\rho))$, the bridge to the gravitational/geometric degrees of freedom $G^{\mu\nu}$, through Einstein's general relativity equations

$$G^{\mu\nu} \equiv R^{\mu\nu} - \frac{1}{2} g^{\mu\nu} R = 8\pi T^{\mu\nu}. \tag{1}$$

For a perfect fluid energy-momentum tensor and for a static spherical symmetric spacetime, the Einstein's field equations lead to the hydrostatic equilibrium equation, well-known as Tolman-Oppenheimer-Volkoff equation [35,36]. This equation reads in natural units

$$p' = -(\rho + p)\frac{4\pi p r + m/r^2}{(1 - 2m/r)}, \tag{2}$$

where the prime indicates radial derivative and m is the gravitational mass enclosed within the surface of radius, i.e.,

$$m' = 4\pi\rho r^2. \tag{3}$$

[1] https://num.pyro.ai

Preprints (www.preprints.org) | NOT PEER-REVIEWED | Posted: 6 May 2022 doi:10.20944/preprints202205.0073.v1

To solve this system one needs to add to it an EoS ($p(\rho)$) and use the boundary conditions

$$m(r)|_{r=0} = 0, \quad p(r)|_{r=0} = p_c \quad \text{and} \quad \rho(r)|_{r=0} = \rho_c, \tag{4}$$

where p_c and ρ_c are the pressure and density at the center of the star. The numerical integration of Eq. (2) follows the pressure decrease as one moves away from the center and it is stopped when the condition

$$p(r)|_{r=R} = 0 \tag{5}$$

is reached at the surface of the star R. The integration of the profile density

$$M(R) \equiv 4\pi \int_0^R r^2 \rho(r) dr \tag{6}$$

provides the total gravitational mass of the star M. The resulting M-R relation can be compared to data from astronomical observations. Once the EoS is provided, the global properties of the neutron stars can be obtained. However, until recently the uncertainties in the mass-radius relationship were significantly large so that almost any EoS could describe the same stellar structure.

The NS can be subdivided in many layers with different theories. Roughly, we can have four regions for the interior: the inner and outer core and the inner and outer crust. For the exterior part, an atmosphere with plasma governed by strong magnetic/electric fields is frequently assumed. The theories to describe the interior span many-body theories of high dense strongly interacting systems, nuclear many-body theories in the high density-temperature regime, atomic structure and plasma physics, respectively [37]. We recall that due to all these different regimes/densities, only the outer crust is well understood, since one can compare with experimental data of atomic nuclei. Around the nuclear saturation density and above, the constraints become too fragile allowing for many descriptions of the NS interior: for the outer core $npe\mu$ (neutron-proton-electron-muon) plasma and for the inner core many possibilities such as fermion/boson condensation, hyperons, pion/kaon condensation, strange quarks surrounded by hadronic matter and so on. This complex puzzle, calls for an extension of our knowledge about the many-body physics regimes and should lead to models able to describe a large variety of environments all at once.

3. The equation of state

The description of the outer crust inside neutron stars is well accepted to be given in terms of hydronic matter up to the saturation density $\rho_0 = 2.8 \times 10^{14}$ g cm^{-3}. This limit reflects the validity of well established nuclear structure models that were developed to describe properties of heavy atomic nuclei on Earth. When one goes beyond ρ_0, more sophisticated degrees of freedom, as mentioned in the previous section, have to be considered. These extra variables make a universal and simultaneously description of systems with such large range density profiles a challenging task. The microscopic constraints are so far just a few and consist of $dp/d\rho$ being always positive and well-defined with $p \geq 0$, electric neutrality, beta equilibrium and the speed of the sound must be less than the speed of light.

Generally speaking, the different set of EoS can be separated accordingly to the compressibility of the nuclear matter: soft and stiff and the corresponding speed of sound. Among the several microscopic methods for the EoS we cite: Perturbation expansions within the Brueckner-Bethe-Goldstone theory, perturbation expansions within the Green's-function theory, variational methods, effective energy-density functionals, and relativistic mean-field (RMF) models [37–42]. Point-coupling and non-relativistic models employing well known nuclear interaction such as Skyrme and Gogny are also used [43–49]. Two approaches are frequently seen in the literature: Models that approach the physics around ρ_0 [50–52]; or models that aim specific systems such as binary neutron star mergers, e.g. using LIGO-VIRGO observational data for the mass-radius of NS to extract the embedded EoS model [53]. In general, the EoS are generated through these models using parameters adjusted to reproduce fundamental physical quantities and are listed in tabulated data, i.e., there are many models and many codes/ways to generate them. The phenomenological models have the advantage of being easily parametrized and can generate EoS that reproduce the M-R diagrams, offering simpler representations of sophistical microscopic calculations. These are the so-called representation of the EoS, which are basically two: the piecewise-polytropic [34,54–58] and spectral representations [59,60]. Here we focus on models of the first kind.

Piecewise-polytropic representation

The piecewise polytropic model consists of a connected set of polytropic equations, effectively power-law like functions, with different exponents (also called indices) to account for the softness/stiffness of the EoS at a given density

Preprints (www.preprints.org) | NOT PEER-REVIEWED | Posted: 6 May 2022 doi:10.20944/preprints202205.0073.v1

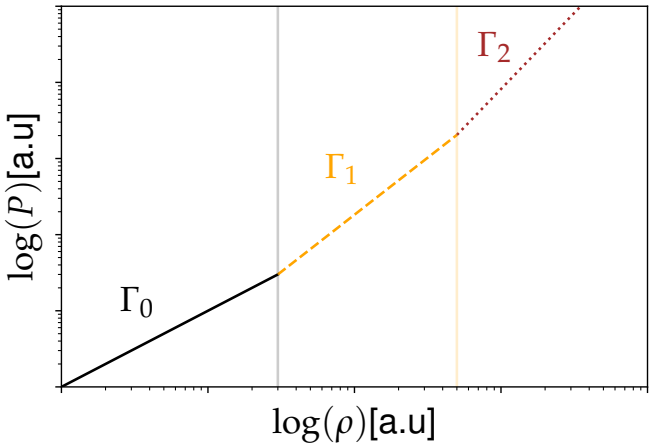

Figure 1. Piecewise model representation of the equations of state with the polytropic equations (7). The vertical lines represent the transition points $\rho_{0\to1}$ and $\rho_{1\to2}$ of each piece of the EoS.

regime. The indices are free parameters in most of the cases when one considers this kind of parametrization. The density where the transition between two polytropic equations take place can also be used as a free parameter specially at highly dense regions [61]. The polytropic representation can yield macroscopic observables for a wide range of EoS with only a few parameters. The stellar structure maps the EoS parameters to gravitational mass, radius, moment of inertia and others global properties. This representation has been extensively used in NS studies, gravitational waves simulations [62–65] and can be tested using the astronomical data such X-ray, gamma and gravitational waveforms. The representations can be also very useful when dealing with modified gravity such as $f(R)$ [66,67] and or other alternative theories where a coupling between geometry and matter could introduce corrections in the energy density, and therefore requires an analytical representation to model the stellar structure [68].

The piecewise-polytropic parametrization of the EoS can be written as [34]

$$P(\rho) = K_i \rho^{\Gamma_i}, \tag{7}$$

where Γ_i are the polytropic indices and K_i strength constants. Due to the continuity of pressure at the transition points, we impose (with $i > 0$)

$$K_i = K_{i-1} \rho_t^{\Gamma_{i-1}-\Gamma_i}. \tag{8}$$

In this work the piecewise polytropic parametrization of the EoS is done by combining three different polytropes. We have two parameters to set the transitions points and three values of Γ for each region. For the first piecewise, i.e, at density values smaller than $\rho_{0\to1}$, see the gray vertical line in Fig. 1, we define Γ_0 (and K_0) in connection to the SLy4 EoS in this regime. This equation of state, describes very well the nuclear matter and match the BPS and HP94 based on experimental nuclear data, e.g., see Fig. 1 of Ref. [69]. We set $\Gamma_0 = 1.475$ and $K_0 = 1.475 \times 10^{-3}$ $[\mathrm{fm}^3/\mathrm{MeV}]^{2/3}$.

The two other polytropic combination of (7) have the set of parameters $\{\Gamma_1, \Gamma_2\}$, and the respective transition taking place at $\rho_{0\to1}$ (see Fig. 1). Having the first part of the EoS fixed the transition point $\rho_{1\to2}$ is placed at two different density values and the exponents $\{\Gamma_1, \Gamma_2\}$ are analyzed with statistical methods in relation to data from astronomical observations.

4. Markov Chain Monte Carlo and Bayesian Inference

Markov Chain Monte Carlo (MCMC) is a convenient numerical way to stochastically explore a space of parameter values with high probability and provides good expectation estimates for model variability. This is basically the point of any Bayesian inference quantification summarized in terms of mean and variance values. One assumes a distribution F for a given parameter with mean value q_t, an associated uncertainty σ_t, and with a transition probability $K(q'|q)$ we can write

$$F(q) = \int dq' F(q') K(q'|q). \tag{9}$$

Preprints (www.preprints.org) | NOT PEER-REVIEWED | Posted: 6 May 2022 doi:10.20944/preprints202205.0073.v1

Since the form of F is preserved, the algorithm can start from any point q' that the convergence to the typical parameter space region is guaranteed. Sampling from a prior distribution F and employing a simple Metropolis algorithm with $t = 0, \ldots, t = T$ iterations to construct the Markov Chain $[q_{t=0}, q_{t=1}, \ldots, q_{t=T}]$ one approximates the posterior distribution given a sufficient large number of steps T. The sampled value q is accepted according to the probability

$$\Pi = \frac{f(\chi^2(q_{t+1}))}{f(\chi^2(q_t))}, \tag{10}$$

where $f(x) = e^{-x}$ and χ^2 are the likelihood and chi-squared functions, respectively. More details and algorithms can be found in Refs [70–72].

Here, we employ the MCMC algorithm to access the variability of polytropic piecewise-like models. The set of parameters are assumed to be uncorrelated and normally distributed. We defined 5 (MD#) models containing different parameterization schemes. The parameters of the first polytrope (left side of the gray vertical line of Fig. 1) is kept unchanged with $\rho_0 \equiv \rho_{0\to1} = 2.8 \times 10^{14}$ g cm^{-3} $= 0.17$ fm^{-3} and $\Gamma_0 = 1.475$. This low density region of the EoS is well understood in terms of hadronic matter. For densities values $\rho_{0\to1} < \rho \leq \rho_{1\to2}$ we use the second polytrope, representing an intermediate high-density portion of the EoS with adiabatic index Γ_1. This segment of the EoS (center part of Fig. 1) is not fully understood with our current knowledge of microphysics, representing a density region where EoS variability can be studied. Finally, the transition to the third polytrope with adiabatic index Γ_2 (right side Fig. 1)) is defined by the density transition region $\rho_{1\to2}$, representing the densest part of the EoS. The value defining the transitions is difficult to be estimated since the physics of highly dense interacting matter is yet not known in details, and therefore it can be arbitrarily chosen.

We worked with two different values for the transition region $\rho_{1\to2} = \{4.8\rho_0; 7.2\rho_0\}$. These two choices will have the two following sets of polytropic indices $\Gamma_1 = \{2.5, 2.6, 2.8, 3.0\}$ and $\Gamma_2 = \{1.8, 1.9, 3.0, 3.3, 3.7\}$ for the polytrope 1 and 2, respectively. Once the transition point $\rho_{1\to2}$, and $\Gamma_{1,2}$ are defined, one can calculate the constant K for each individual polytrope using Eq. (8) and have the full the description of the EoS.

In total, we have 5 combinations of parameters schemes. Our MD#s, provide a large variety of equation of states, i.e. different densities and pressure profiles to be used in solving the TOV equation, and generating the respective stellar global properties. Our models are summarized in Table 1, where the color scheme used in the figures is also provided.

Label	$\rho_{1\to2}$	Γ_1	Γ_2	Color
MD1	$7.2\rho_0$	2.5	1.8	cyan
MD2	$7.2\rho_0$	2.6	1.9	pink
MD3	$4.8\rho_0$	2.6	3.0	purple
MD4	$4.8\rho_0$	2.8	3.3	brown
MD5	$4.8\rho_0$	3.0	3.7	lime

Table 1: Summary of the parameters for piecewise EoS models. $\rho_0 = 2.8 \times 10^{14}$ g cm^{-3} $= 0.17$ fm^{-3} is the nuclear saturation density. We assumed the uncertainty as $\sigma = 0.01$ for both $\Gamma_{1,2}$ in each model.

The MCMC is applied for Γ_1 and Γ_2 with an error uncertainty of $\sigma = 0.01$ associated to each of the exponents. All the other parameters are kept fixed. Small variations in the polytropic indices lead to large change in the pressure, specially at density regimes of $> 4\rho_0$. Therefore, the variation of $\Gamma_{1,2}$ provides a way to access the impact of EoS variability on the mass radius diagram for the models employed here.

Figure 2 presents the posterior distributions of values obtained in the MCMC process for the exponents Γ_1 and Γ_2 in the left and right panels, respectively. We employ $N = 10000$ iterations of the Monte Carlo sampling for each of the models defined in Table 1. This number of steps ensure convergence of the posterior distribution presented as histograms. Figures 2(a-b) represent the model MD1 with averaged values for $\langle\Gamma_1\rangle = 2.5$ and $\langle\Gamma_2\rangle = 1.8$. The histograms for the parameters of MD2 is shown in Figs 2(c-d) with $\langle\Gamma_1\rangle = 2.6$ and $\langle\Gamma_2\rangle = 1.9$. The corresponding histogram with averaged values $\langle\Gamma_1\rangle = 2.6$ and $\langle\Gamma_2\rangle = 3.0$ for model MD3 is shown in Figs 2(e-f).

The two last subfigures of Fig. 2, Figs 2(g-h) and Figs 2(i-j), are associated to models MD4 and MD5 respectively. MD4 has the averaged values of $\langle\Gamma_1\rangle = 2.80$ and $\langle\Gamma_2\rangle = 3.30$. For the MD5, we have the following ones $\langle\Gamma_1\rangle = 3.00$ and $\langle\Gamma_2\rangle = 3.70$. The averaged value of each distribution confirms the convergence of the statistical sampling approach.

The MCMC provides the posterior distribution for what we can sample $\Gamma_{1,2}$ values to generate equation of states for each of the model MD#. The EoS is then used to solve the TOV equation to obtain the mass and radius diagrams. As

Preprints (www.preprints.org) | NOT PEER-REVIEWED | Posted: 6 May 2022 doi:10.20944/preprints202205.0073.v1

we are going to see the MD4 and MD5 are the representations that seem to better reproduce the EoS, according to the observations.

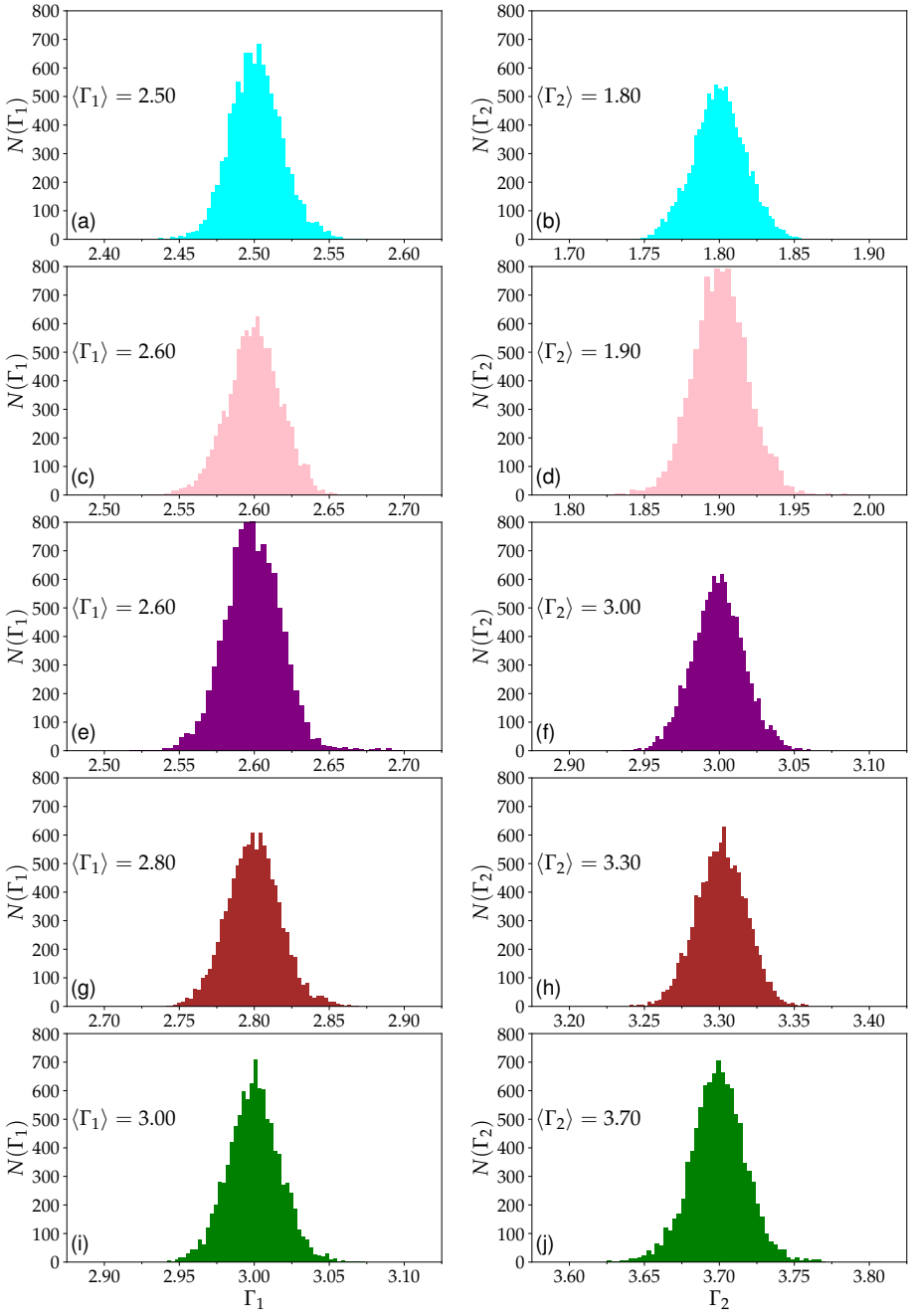

Figure 2. Histograms for MCMC sampling for the five models: MD1, MD2, MD3, MD4 and MD5 (from top to bottom). The distributions are obtained with 10000 iterations. The averaged values for each histogram is shown in the inset and match the parameters given Table 1.

In figure 3 we have the parametrized EoS for each model of 5 models studied here. As one can see, at low densities they all converge to a single picture determined by the SLy4 parametrization. At higher densities they diverge from each other, where the MD1 being the softest model and the MD5 the stiffest one. The parametrization of MD1 and MD2 in the third polytrope, Γ_2, reduces the speed of sound, which reflects a decrement in comparison with the other models for higher densities. This feature will be reflected in the mass-radius diagram, as we are going to see.

Preprints (www.preprints.org) | NOT PEER-REVIEWED | Posted: 6 May 2022 doi:10.20944/preprints202205.0073.v1

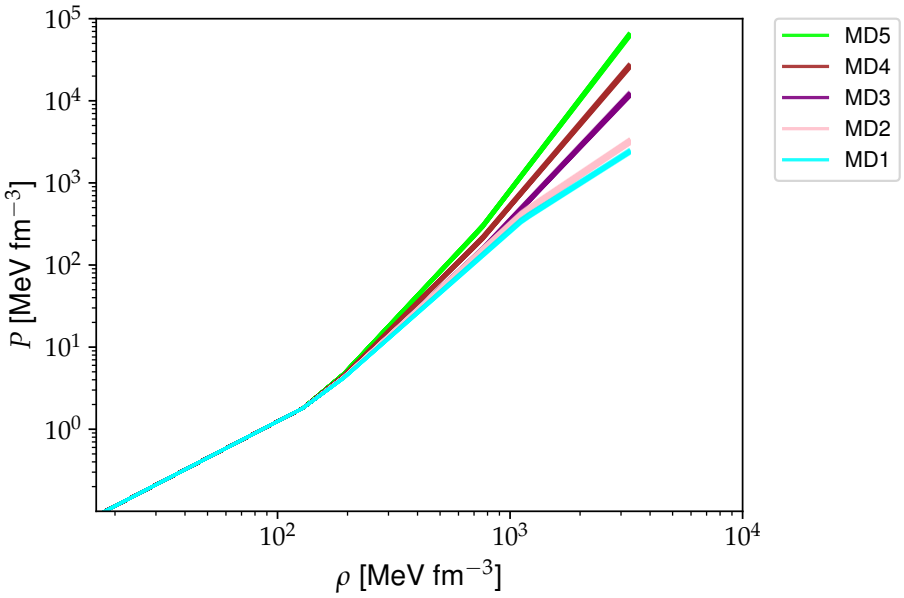

Figure 3. The collection of EoS generated for the 5 models defined in Table 1. The description of the regime of low density associated to the nuclear matter saturation point ρ_0 is kept unchanged for every model. The transition between different polytropic equation can be seen as elbows with large Γ values providing highly stiff equation of state.

In Figure 4 we present the mass-radius relation for the 5 sets of our EoS parametrization. They are respectively the models going from 1 to 5 in table 1. In this figure we also have the LIGO-VIRGO mass-radius region, in blue and orange, constrained by the gravitational wave event GW170817 [6,73], This constraint was the first one to have a radius associated with the mass tightly constrained, since the previous observations for neutron stars were using electromagnetic bandwidth, which is very difficult to estimate the radius of NS. After this gravitational wave detection, the radius of a pure nuclear hadronic matter with mass of 1.4 $M_\odot$ was estimated to be $\overline{R}_{1.4}$ = 12.39 km [74]. Afterwards, this constraint was shifted due to measurements of *NICER* for the pulsar PSR J0030+0451 to two values: $M \approx 1.44\ M_\odot$ and equatorial radius of $R_{\rm eq} = 13.02$ km [17] and $M \approx 1.24\ M_\odot$ and $R_{\rm req} = 12.71$ km [18]. This information is highlighted by the black dots with error bars in the mass-radius diagram. In Fig. 4 we present as upper limit of mass, a lower mass compact object with $2.50 - 2.67\ M_\odot$ in a binary system detected by LIGO-VIRGO [75], this unknown object if it is a NS, will be a breakthrough, since no nuclear theory for ordinary matter, can explain such a EoS to generate such a mass in general relativity. Finally, we considered observations of massive pulsars: The extremely massive millisecond pulsar PSR J0740+6620 with mass of $2.14^{+0.20}_{-0.18}\ M_\odot$ [76]; the PSR J2215+5135 with mass $\approx 2.27\ M\odot$ [77]. The measurement of the mass of the source is not so precise, and if this number is confirmed, the star would be the most massive neutron star ever detected; the two well-known NS sources J0348+0432 and J1614-2230 [78,79] with $M = 2.0\ M_\odot$.

As we can see in the mass-radius diagram, the models MD4 and MD5, brown and lime curves respectively, seem to better explain the observation. One can see that the curves cross the region of the *NICER* observation. For the mass of 1.4 $M_\odot$, the respective radius for MD4 and MD5 are: $\overline{R}_{\rm MD4} = 11.96$ km and $\overline{R}_{\rm MD5} = 12.44$ km, the other models for the same mass are more compact and are off the *NICER* data, although they are still inside the LIGO-VIRGO region. These two approaches also cross the line for $M = 2.0\ M_\odot$ pulsars as well as they are inside the region for PSR J0740+6620 and PSR J2215+5135 mass. Regarding the model MD5, even the compact object with 2.5 $M_\odot$ could be explained with this parametrization. They have as maximum mass $\overline{M}_{\rm max\ MD4} = 2.35\ M_\odot$ and $\overline{M}_{\rm max\ MD5} = 2.57\ M_\odot$ and respective radius $\overline{R}_{\rm MD4} = 9.63$ km and $\overline{R}_{\rm MD5} = 10.21$ km.

Concerning the model MD3, the purple one, it could explain the massive pulsars also; however, it starts to get out of the *NICER* constraints. In this region of mass-radius this parametrization mixes with the model MD2, the pink one. They have similar Γ_1, which reflects in the central density when solving the TOV equation and getting the mass of the star in this region. For the densest region, the model MD2 can barely reach the two solar mass region. It has a maximum mass of $\overline{M}_{\rm max\ MD2} = 1.97\ M_\odot$ and radius of $\overline{R}_{\rm MD2} = 9.49$ km. For the model MD1, one cannot have the stars with mass close to two solar masses, and it lies away of the *NICER* measurement.

Preprints (www.preprints.org) | NOT PEER-REVIEWED | Posted: 6 May 2022 doi:10.20944/preprints202205.0073.v1

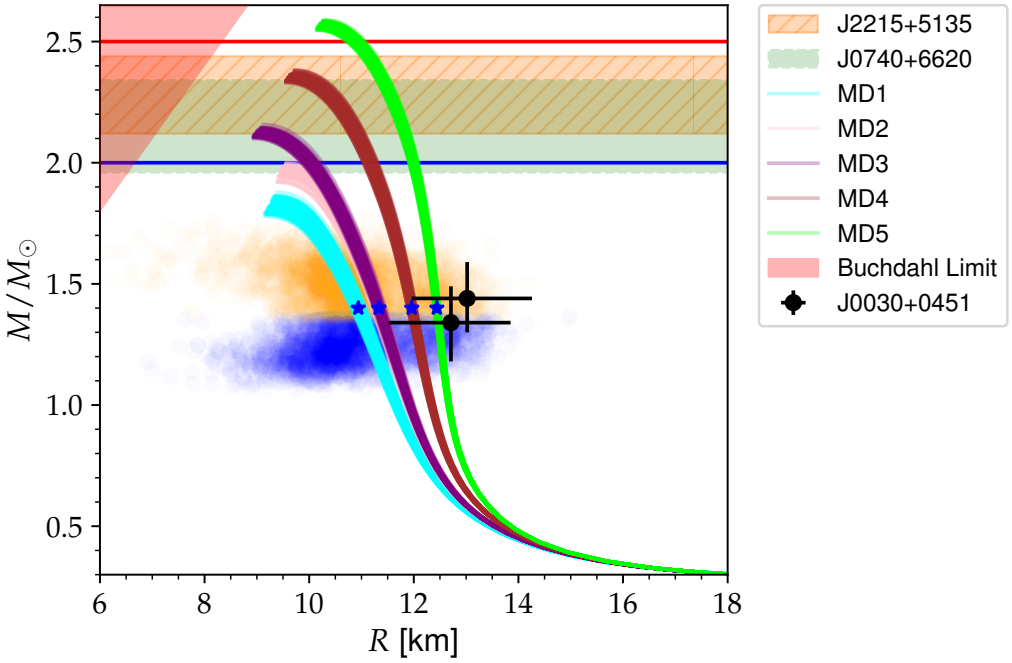

Figure 4. Mass radius relationship for the set of all our parametrizations. We have five lines corresponding to the MD#s in table 1. The blue continuous line at 2.0 $M_\odot$ corresponds to the two massive pulsars J0348+0432 and J1614-2230. The filled green region represents the pulsar J0740+6620 and the filled dashed salmon region is the pulsar J2215+5135. The red line is the low mass compact object in the binary system GW190414. The black dots with errors bars are the *NICER* estimations of PSR J0030+0451. The blue solid stars mark 1.4 $M_\odot$ stars.

5. Bayesian Power Regression Model with Heteroscedastic errors

In this section, we briefly investigate the potential use of a Bayesian Power Regression model with heteroscedastic errors (BPR-HE) to capture the relationship between the density and pressure. The idea here is to train a model that incorporates the associated variance of a large variety of physics parameterization. This approach could then be constrained by observational data automatically in a physics informed machine learning strategy. As a preliminary step towards that, we focus in the BPR-HE approach.

Power regression is a non-linear regression model that take the form $y = ax^b$, where y is the response variable, x is the prediction variable, and a and b are the coefficients that describe the relationship between x and y. The model can be made linear by simply applying a log transformation: $\log(y) = \log(a) + b\log(x)$. Therefore, one can infer the parameters of a non-linear power regression model via a linear model. With that, our corresponding BPR-HE model is defined as

$$\begin{aligned} \log(p^i) &\sim \text{Normal}(\alpha \cdot \log(\rho^i) + \beta, s_m \cdot \log(\rho^i) + s_b), \qquad \forall i = 1, ..., N. \\ \alpha &\sim \text{Normal}(\gamma_1, \gamma_2) \\ \beta &\sim \text{Normal}(0, \gamma_3) \\ s_m &\sim \text{HalfCauchy}(\gamma_4) \\ s_b &\sim \text{HalfCauchy}(\gamma_5) \end{aligned} \tag{11}$$

where γ_* are a set of hyper-parameters that are specified by the user. In our experiment, we set all γ to 1. N = 65 is the total number of equation of states taken from the LIGO *Lalsuite* [80] library and used as data set. Essential to the model is the dependence of the standard deviation of the residual to the density variable ρ. This is necessary as the ensemble of EoS from LiGO have an increasing pressure variance with respect to densities. Residuals with varying variance is known as heteroscedastic. Figure 5 shows an illustrative example of heteroscedastic errors and homoscedastic errors, which is assumed in classical linear regression models.

We used the Numpyro probabilistic programming language [81] to implement the model 11. We inferred the values of the unknown parameters in our model (α, β, s_m, and s_b) by running MCMC using the No-U-Turn Sampler (NUTS) [82] for 10000 warm-up samples and then collected 1000 posterior samples to represent our model parameters posterior distribution.

Preprints (www.preprints.org) | NOT PEER-REVIEWED | Posted: 6 May 2022 doi:10.20944/preprints202205.0073.v1

Figure 6 shows posterior samples of the BPR-HE model (in yellow), and the EoS from LIGO. Notice that the model captures the increasing variance of the pressure as the density increases. This is due to the heteroscedastic errors in the model. The BPR-HE provides smooth functions as opposed to the piecewise polytropic approach described in the previous section. The abrupt transition points of the MD# models can reduce the accuracy of the description of local speed of sound, a problem already discussed in [34].

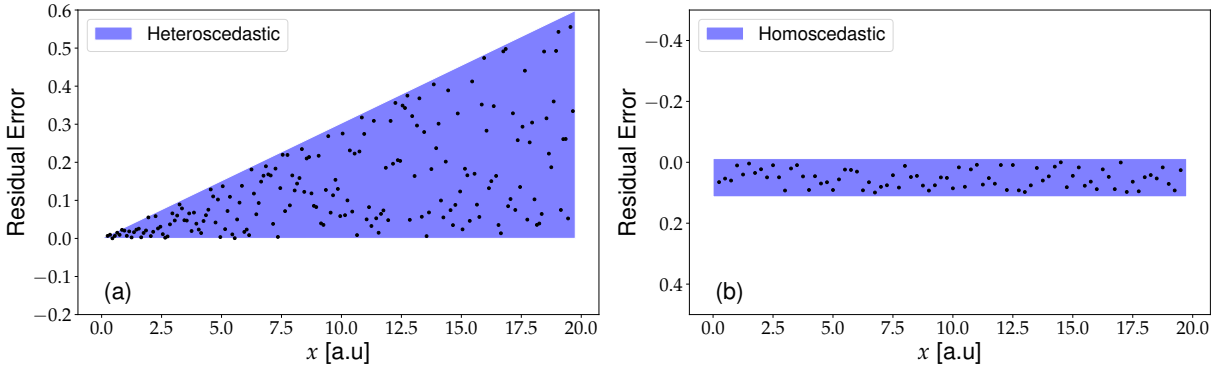

Figure 5. Representative example of heteroscedastic (a) and homoscedastic (b) residuals. Notice how the variance of the residuals changes with the value of x for the first, while it remains constant for the second.

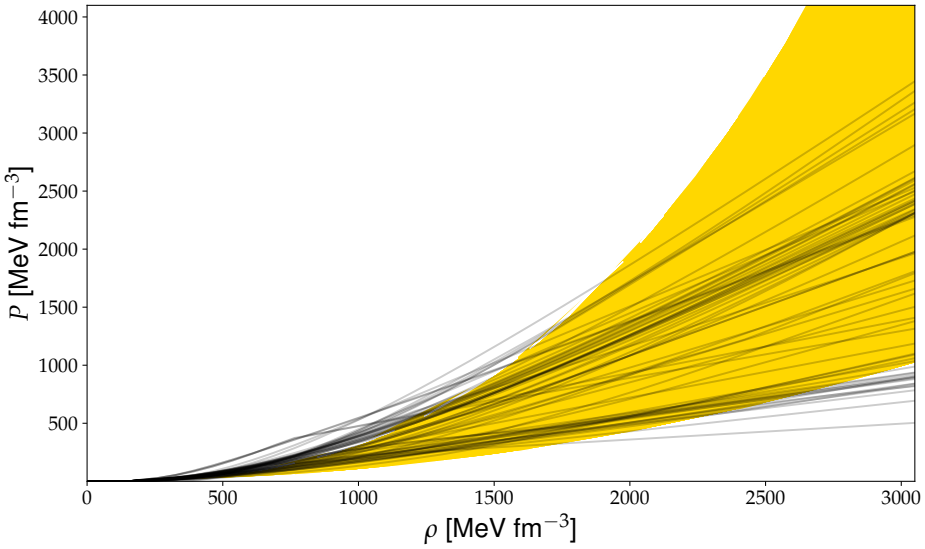

Figure 6. Bayesian Power Regression model heteroscedastic errors. Black solid lines are the 65 EoS from the LIGO *Lalsuite* [80] data set, while the yellow ones are posterior samples generated by the BPR-HE model.

From Figure 6, we observe that the BPR-HE model is a promising approach to be used to model the relation of density and pressure. This information can be used to estimate uncertainties of the maximum radius and mass of the neutron stars via TOV equations. We left the use of BPR-HE generated EoS into the TOV equation for future works and have restricted this work to a feasibility analysis of such approach.

6. Conclusion and perspectives

In this paper, we have studied parameters of piecewise polytropic equations that are representative of an equation of state modeling the interior structure of neutron stars. Polytropic piecewise models with few parameters are known to be good approximations to modern theoretical EoS and are able to reproduce global features of neutron stars such as mass, radius, moment of inertia and so on (e.g. see Ref. [26,34,53,58,83,84]). Commonly used in literature, this phenomenological approach is applied in a broad research context from numerical solution of rotating relativistic stars/merger simulations [65,85,86] to modified gravity [66,68,87–89] studies. Also recently, they have successfully been applied to constrain the dense matter equation of state of neutron stars supported by observations [53,90–92].

In this work, we have connected three politropes resulting in 5 different schemes globally adjusted. We performed an analysis that have accounted for different astronomical observational sources, in a joint constraint. We have performed a Bayesian analysis of piecewise equations and then Markov Chain Monte Carlo (MCMC) strategies were we employed to access the variability of our models to constrain the representation of the EoS compared with observations of neutron stars. We have obtained 2500 mass-radius diagrams within the 5 different model schemes. The massive stars $M > 2M_\odot$ and stars with mass around $M \approx 2M_\odot$ can be explained with combinations of adiabatic indices of $2.8 \lessapprox \Gamma_{1,2} \lessapprox 3.7$, as in the case of MD4 and MD5. Increasing this exponent even further will stiff more the EoS and result in unrealistic stars.

From our adopted schemes, the two models, MD4 and MD5, can represent very well stars for mass around 1.4 $M_\odot$ and radius of $\approx$ 12 km, i.e., the mass-radius observational region of LIGO-VIRGO binary NS merger and the PSR J0030+0451 constrained by the *NICER* experiment. The two models can also explain massive pulsars with mass above 2.0 $M_\odot$ as the two pulsars J0348+0432 and J1614-2230. One of the models, MD5, can even explain an unknown object with mass of 2.5 $M_\odot$ in a binary system, detected by LIG0-VIRGO. This model has a maximum mass of $\overline{M} = 2.57\ M_\odot$. As one can notice, the model MD5 yields almost the same radius for different masses, almost a limit for the polytropic exponent.

The parameters found here for the piecewise equations that represent modern EoS, will be used to constraint nuclear models, i.e., the parameters of many-body models. In previous works [93,94], we analyzed correlations in the microphysics of many EoS and in the global properties. We have studied two separated spaces, and now we are able to bring these two complementary studies together in a full picture and by means of statistical and machine learning tools, shading light in the path to understand the EoS of neutron stars.

Before closing, we would like to comment on some challenges and remarks on modeling EoS coming from many nuclear models with different parametrizations. Statistical models, such as regression model with heteroscedastic errors, for example, has the potential to best represent a set of different physics included in a variety of equation of states. The Bayesian Power Regression model with heteroscedastic errors (BPR-HE) is a flexible model, but we faced difficulties with it due to the nature of the data. In the model, the variance of the errors varies linearly with the density value, which might not be appropriate, as the s_m parameter has shown to be very sensitive and difficult to infer. We had to resort to a forceful (informative) prior to stabilize the inference. Another point is that using a single power regression model to describe all EoS might be too restrictive, given the diversity of physical models. We believe that a mixture regression model, composed of several power regressors, will bring more flexibility. These points will be the focus of future research steps, as well the tension brought by the Lead Radius EXperiment (PREX-2) results with astronomical data.

Funding: This research was partly funded by U.S. Department of Energy (DOE) under grant DE–FG02–08ER41533 and to the LANL Collaborative Research Program by Texas A&M System National Laboratory Office and Los Alamos National Laboratory. Also, partly funded by UNIANDES University.

Data Availability Statement: This is a theoretical work and the data used are public in the cited and respective references.

Acknowledgments: We acknowledge the organizers of the conference “The Modern Physics of Compact Stars and Relativistic Gravity 2021” and Prof. Sedrakian, the editor of the special issue "Selected Papers from “The Modern Physics of Compact Stars and Relativistic Gravity 2021”" for the contribution invite.

Conflicts of Interest: The authors declare no conflict of interest.

References

1. Hewish, A.; Bell, S.J.; Pilkington, J.D.H.; Scott, P.F.; Collins, R.A. Observation of a Rapidly Pulsating Radio Source. *Nature* **1968**, *217*, 709. doi:10.1038/217709a0.
2. Radice, D.; Perego, A.; Zappa, F.; Bernuzzi, S. GW170817: Joint Constraint on the Neutron Star Equation of State from Multimessenger Observations. *The Astrophysical Journal Letters* **2018**, *852*, L29. doi:10.3847/2041-8213/aaa402.
3. LIGO Scientific Collaboration and Virgo Collaboration.; et al. Gravitational Waves and Gamma-Rays from a Binary Neutron Star Merger: GW170817 and GRB 170817A. *The Astrophysical Journal* **2017**, [1710.05834]. doi:10.3847/2041-8213/aa920c.
4. LIGO Scientific Collaboration and Virgo Collaboration.; et al. GW170817: Observation of Gravitational Waves from a Binary Neutron Star Inspiral. *Physical Review Letters* **2017**, *119*, 161101, [1710.05836]. doi:10.1103/physrevlett.119.161101.
5. Bauswein, A.; Just, O.; Janka, H.T.; Stergioulas, N. Neutron-Star Radius Constraints from GW170817 and Future Detections. *The Astrophysical Journal* **2017**, *850*, L34. doi:10.3847/2041-8213/aa9994.
6. The LIGO Scientific Collaboration and the Virgo Collaboration.; Abbott. GW170817: Measurements of Neutron Star Radii and Equation of State. *Physical Review Letters* **2018**, *121*, 161101, [1805.11581]. doi:10.1103/physrevlett.121.161101.
7. De, S.; Finstad, D.; Lattimer, J.M.; Brown, D.A.; Berger, E.; Biwer, C.M. Tidal Deformabilities and Radii of Neutron Stars from the Observation of GW170817. *Physical Review Letters* **2018**, *121*, 091102. doi:10.1103/physrevlett.121.091102.
8. Margalit, B.; Metzger, B.D. Constraining the Maximum Mass of Neutron Stars from Multi-messenger Observations of GW170817. *The Astrophysical Journal Letters* **2017**, *850*, L19. doi:10.3847/2041-8213/aa991c.

9. Gamba, R.; Read, J.S.; Wade, L.E. The Impact of the Crust Equation of State on the Analysis of GW170817. *Classical and Quantum Gravity* **2019**, *37*, 025008. doi:10.1088/1361-6382/ab5ba4.
10. Motta, T.F.; Kalaitzis, A.M.; Antić, S.; Guichon, P.A.M.; Stone, J.R.; Thomas, A.W. Isovector Effects in Neutron Stars, Radii, and the GW170817 Constraint. *The Astrophysical Journal* **2019**, *878*, 159. doi:10.3847/1538-4357/ab218e.
11. Lourenço, O.; Dutra, M.; Lenzi, C.H.; Biswal, S.K.; Bhuyan, M.; Menezes, D.P. Consistent Skyrme Parametrizations Constrained by GW170817. *The European Physical Journal A* **2020**, *56*, 32. doi:10.1140/epja/s10050-020-00040-z.
12. Essick, R.; Landry, P.; Holz, D.E. Nonparametric Inference of Neutron Star Composition, Equation of State, and Maximum Mass with GW170817. *Physical Review D* **2020**, *101*, 063007. doi:10.1103/physrevd.101.063007.
13. Tews, I.; Margueron, J.; Reddy, S. Critical Examination of Constraints on the Equation of State of Dense Matter Obtained from GW170817. *Physical Review C* **2018**, *98*, 045804. doi:10.1103/physrevc.98.045804.
14. Lim, Y.; Holt, J.W. Neutron Star Tidal Deformabilities Constrained by Nuclear Theory and Experiment. *Physical Review Letters* **2018**, *121*, 062701. doi:10.1103/PhysRevLett.121.062701.
15. Traversi, S.; Char, P.; Pagliara, G. Bayesian Inference of Dense Matter Equation of State within Relativistic Mean Field Models Using Astrophysical Measurements. *The Astrophysical Journal* **2020**, *897*, 165. doi:10.3847/1538-4357/ab99c1.
16. Gendreau, K.C.; et al.. The Neutron Star Interior Composition Explorer (NICER): Design and Development. *Space Telescopes and Instrumentation 2016: Ultraviolet to Gamma Ray* **2016**, *9905*, 99051H. doi:10.1117/12.2231304.
17. Miller, M.C.; Lamb, F.K.; Dittmann, A.J.; Bogdanov, S.; Arzoumanian, Z.; Gendreau, K.C.; Guillot, S.; Harding, A.K.; Ho, W.C.G.; Lattimer, J.M.; Ludlam, R.M.; Mahmoodifar, S.; Morsink, S.M.; Ray, P.S.; Strohmayer, T.E.; Wood, K.S.; Enoto, T.; Foster, R.; Okajima, T.; Prigozhin, G.; Soong, Y. PSR J0030$\mathplus$0451 Mass and Radius from NICER Data and Implications for the Properties of Neutron Star Matter. *The Astrophysical Journal* **2019**, *887*, L24. doi:10.3847/2041-8213/ab50c5.
18. Riley, T.E.; Watts, A.L.; Bogdanov, S.; Ray, P.S.; Ludlam, R.M.; Guillot, S.; Arzoumanian, Z.; Baker, C.L.; Bilous, A.V.; Chakrabarty, D.; Gendreau, K.C.; Harding, A.K.; Ho, W.C.G.; Lattimer, J.M.; Morsink, S.M.; Strohmayer, T.E. A NICER View of PSR J0030$\mathplus$0451: Millisecond Pulsar Parameter Estimation. *The Astrophysical Journal* **2019**, *887*, L21. doi:10.3847/2041-8213/ab481c.
19. Fujimoto, Y.; Fukushima, K.; Murase, K. Mapping Neutron Star Data to the Equation of State Using the Deep Neural Network. *Physical Review D* **2020**, *101*, 054016. doi:10.1103/physrevd.101.054016.
20. Morawski, F.; Bejger, M. Neural Network Reconstruction of the Dense Matter Equation of State Derived from the Parameters of Neutron Stars. *Astronomy & Astrophysics* **2020**, *642*, A78. doi:10.1051/0004-6361/202038130.
21. Krastev, P.G. Translating Neutron Star Observations to Nuclear Symmetry Energy via Artificial Neural Networks. *arXiv e-prints* **2021**, [2112.04089].
22. Soma, S.; Wang, L.; Shi, S.; Stöcker, H.; Zhou, K. Neural Network Reconstruction of the Dense Matter Equation of State from Neutron Star Observables. *arXiv e-prints* **2022**, [2201.01756].
23. Krastev, P.G. Translating Neutron Star Observations to Nuclear Symmetry Energy via Deep Neural Networks. *Galaxies* **2022**, *10*, 16. doi:10.3390/galaxies10010016.
24. Alford, M.G.; Schmitt, A.; Rajagopal, K.; Schäfer, T. Color superconductivity in dense quark matter. *Rev. Mod. Phys.* **2008**, *80*, 1455–1515. doi:10.1103/RevModPhys.80.1455.
25. Weber, F. Strange quark matter and compact stars. *Progress in Particle and Nuclear Physics* **2005**, *54*, 193–288.
26. Kurkela, A.; Fraga, E.S.; Schaffner-Bielich, J.; Vuorinen, A. Constraining neutron star matter with Quantum Chromodynamics. *Astrophys. J.* **2014**, *789*, 127, [arXiv:astro-ph.HE/1402.6618]. doi:10.1088/0004-637X/789/2/127.
27. Gorda, T.; Kurkela, A.; Romatschke, P.; Säppi, S.; Vuorinen, A. Next-to-Next-to-Next-to-Leading Order Pressure of Cold Quark Matter: Leading Logarithm. *Phys. Rev. Lett.* **2018**, *121*, 202701. doi:10.1103/PhysRevLett.121.202701.
28. Zhou, E.P.; Zhou, X.; Li, A. Constraints on interquark interaction parameters with GW170817 in a binary strange star scenario. *Phys. Rev. D* **2018**, *97*, 083015. doi:10.1103/PhysRevD.97.083015.
29. Li, A.; Zhu, Z.Y.; Zhou, E.P.; Dong, J.M.; Hu, J.N.; Xia, C.J. Neutron star equation of state: Quark mean-field (QMF) modeling and applications. *Journal of High Energy Astrophysics* **2020**, *28*, 19–46.
30. Miller, M.C.; Chirenti, C.; Lamb, F.K. Constraining the Equation of State of High-density Cold Matter Using Nuclear and Astronomical Measurements. *The Astrophysical Journal* **2019**, *888*, 12. doi:10.3847/1538-4357/ab4ef9.
31. Sedaghat, J.; Zebarjad, S.M.; Bordbar, G.H.; Panah, B.E.; Moradi, R. Is the compact binary coalescence, GW190425, a strange quark star?, 2021. doi:10.48550/arxiv.2104.00544.
32. Miao, Z.; Jiang, J.L.; Li, A.; Chen, L.W. Bayesian Inference of Strange Star Equation of State Using the GW170817 and GW190425 Data. *The Astrophysical Journal Letters* **2021**, *917*, L22. doi:10.3847/2041-8213/ac194d.
33. Traversi, Silvia.; Char, Prasanta.; Pagliara, Giuseppe.; Drago, Alessandro. Speed of sound in dense matter and two families of compact stars. *A&A* **2022**, *660*, A62. doi:10.1051/0004-6361/202141544.
34. Read, J.S.; Lackey, B.D.; Owen, B.J.; Friedman, J.L. Constraints on a Phenomenologically Parametrized Neutron-Star Equation of State. *Physical Review D* **2009**, *79*, 124032. doi:10.1103/physrevd.79.124032.
35. Tolman, R.C. Static Solutions of Einstein's Field Equations for Spheres of Fluid. *Physical Review* **1939**, *55*, 364–373. doi:10.1103/physrev.55.364.
36. Oppenheimer, J.R.; Volkoff, G.M. On Massive Neutron Cores. *Physical Review* **1939**, *55*, 374–381. doi:10.1103/physrev.55.374.

37. Haensel, P.; Potekhin, A.Y.; Yakovlev, D.G. *Neutron Stars 1: Equation of State and Structure*; Astrophysics and Space Science Library, Neutron Stars, Springer-Verlag: New York, 2007. doi:10.1007/978-0-387-47301-7.
38. Bethe, H.A. Theory of Nuclear Matter. *Annual Review of Nuclear Science* **1971**, *21*, 93–244. doi:10.1146/annurev.ns.21.120171.000521.
39. Ring, P.; Schuck, P. *The Nuclear Many-Body Problem*; Theoretical and Mathematical Physics, The Nuclear Many-Body Problem, Springer-Verlag: Berlin Heidelberg, 1980.
40. Blaizot, J.P.; Ripka, G. *Quantum Theory of Finite Systems*; The MIT Press: Cambridge, Mass, 1985.
41. Machleidt, R. The Meson Theory of Nuclear Forces and Nuclear Structure. In *Advances in Nuclear Physics*; Negele, J.W.; Vogt, E., Eds.; Advances in Nuclear Physics, Springer US: Boston, MA, 1989; pp. 189–376. doi:10.1007/978-1-4613-9907-0_2.
42. Akmal, A.; Pandharipande, V.R. Spin-Isospin Structure and Pion Condensation in Nucleon Matter. *Physical Review C* **1997**, *56*, 2261–2279. doi:10.1103/physrevc.56.2261.
43. Nikolaus, B.A.; Hoch, T.; Madland, D.G. Nuclear Ground State Properties in a Relativistic Point Coupling Model. *Physical Review C* **1992**, *46*, 1757–1781. doi:10.1103/physrevc.46.1757.
44. Friar, J.L.; Madland, D.G.; Lynn, B.W. QCD Scales in Finite Nuclei. *Physical Review C* **1996**, *53*, 3085–3087. doi:10.1103/physrevc.53.3085.
45. Skyrme, T.H.R. The Effective Nuclear Potential. *Nuclear Physics* **1958**, *9*, 615–634. doi:10.1016/0029-5582(58)90345-6.
46. Bell, J.S.; Skyrme, T.H.R. CVIII. The Nuclear Spin-Orbit Coupling. *The Philosophical Magazine: A Journal of Theoretical Experimental and Applied Physics* **1956**, *1*, 1055–1068. doi:10.1080/14786435608238187.
47. Skyrme, T.H.R. CVII. The Nuclear Surface. *Philosophical Magazine* **2006**. doi:10.1080/14786435608238186.
48. Dechargé, J.; Gogny, D. Hartree-Fock-Bogolyubov Calculations with the $D1$ Effective Interaction on Spherical Nuclei. *Physical Review C* **1980**, *21*, 1568–1593. doi:10.1103/physrevc.21.1568.
49. Berger, J.F.; Girod, M.; Gogny, D. Time-Dependent Quantum Collective Dynamics Applied to Nuclear Fission. *Computer Physics Communications* **1991**, *63*, 365–374. doi:10.1016/0010-4655(91)90263-k.
50. Dutra, M.; Lourenço, O.; Sá Martins, J.S.; Delfino, A.; Stone, J.R.; Stevenson, P.D. Skyrme Interaction and Nuclear Matter Constraints. *Physical Review C* **2012**, *85*, 035201. doi:10.1103/physrevc.85.035201.
51. Dutra, M.; Lourenço, O.; Avancini, S.S.; Carlson, B.V.; Delfino, A.; Menezes, D.P.; Providência, C.; Typel, S.; Stone, J.R. Relativistic Mean-Field Hadronic Models under Nuclear Matter Constraints. *Physical Review C* **2014**, *90*, 055203. doi:10.1103/physrevc.90.055203.
52. Lourenço, O.; Dutra, M.; Lenzi, C.H.; Flores, C.V.; Menezes, D.P. Consistent Relativistic Mean-Field Models Constrained by GW170817. *Physical Review C* **2019**, *99*, 045202. doi:10.1103/physrevc.99.045202.
53. Miao, Z.; Jiang, J.L.; Li, A.; Chen, L.W. Bayesian Inference of Strange Star Equation of State Using the GW170817 and GW190425 Data. *The Astrophysical Journal Letters* **2021**, *917*, L22. doi:10.3847/2041-8213/ac194d.
54. Mueller, E.; Eriguchi, Y. Equilibrium Models of Differentially Rotating, Completely Catalyzed, Zero-Temperature Configurations with Central Densities Intermediate to White Dwarf and Neutron Star Densities. *Astronomy and Astrophysics* **1985**, *152*, 325–335.
55. Hebeler, K.; Lattimer, J.M.; Pethick, C.J.; Schwenk, A. Constraints on Neutron Star Radii Based on Chiral Effective Field Theory Interactions. *Physical Review Letters* **2010**, *105*, 161102. doi:10.1103/PhysRevLett.105.161102.
56. Steiner, A.W.; Lattimer, J.M.; Brown, E.F. THE EQUATION OF STATE FROM OBSERVED MASSES AND RADII OF NEUTRON STARS. *The Astrophysical Journal* **2010**, *722*, 33. doi:10.1088/0004-637X/722/1/33.
57. Özel, F.; Psaltis, D.; Güver, T.; Baym, G.; Heinke, C.; Guillot, S. THE DENSE MATTER EQUATION OF STATE FROM NEUTRON STAR RADIUS AND MASS MEASUREMENTS. *The Astrophysical Journal* **2016**, *820*, 28. doi:10.3847/0004-637X/820/1/28.
58. Raithel, C.A.; Özel, F.; Psaltis, D. From Neutron Star Observables to the Equation of State. I. An Optimal Parametrization. *The Astrophysical Journal* **2016**, *831*, 44. doi:10.3847/0004-637x/831/1/44.
59. Lindblom, L.; Indik, N.M. Spectral Approach to the Relativistic Inverse Stellar Structure Problem. *Physical Review D* **2012**, *86*, 084003. doi:10.1103/PhysRevD.86.084003.
60. Lindblom, L.; Indik, N.M. Spectral Approach to the Relativistic Inverse Stellar Structure Problem II. *Physical Review D* **2014**, *89*, 064003. doi:10.1103/PhysRevD.89.064003.
61. Özel, F.; Psaltis, D. Reconstructing the Neutron-Star Equation of State from Astrophysical Measurements. *Physical Review D* **2009**, *80*, 103003. doi:10.1103/PhysRevD.80.103003.
62. Lackey, B.D.; Wade, L. Reconstructing the Neutron-Star Equation of State with Gravitational-Wave Detectors from a Realistic Population of Inspiralling Binary Neutron Stars. *Physical Review D* **2015**, *91*, 043002. doi:10.1103/physrevd.91.043002.
63. Carney, M.F.; Wade, L.E.; Irwin, B.S. Comparing Two Models for Measuring the Neutron Star Equation of State from Gravitational-Wave Signals. *Physical Review D* **2018**, *98*, 063004. doi:10.1103/physrevd.98.063004.
64. Ma, P.X.; Jiang, J.L.; Wang, H.; Jin, Z.P.; Fan, Y.Z.; Wei, D.M. GW170817 and the Prospect of Forming Supramassive Remnants in Neutron Star Mergers. *The Astrophysical Journal* **2018**, *858*, 74. doi:10.3847/1538-4357/aabafe.
65. East, W.E.; Paschalidis, V.; Pretorius, F.; Tsokaros, A. Binary Neutron Star Mergers: Effects of Spin and Post-Merger Dynamics. *Physical Review D* **2019**, *100*, 124042. doi:10.1103/physrevd.100.124042.
66. Astashenok, A.V.; Capozziello, S.; Odintsov, S.D. Further Stable Neutron Star Models from f (R) Gravity. *Journal of Cosmology and Astroparticle Physics* **2013**, *2013*, 040. doi:10.1088/1475-7516/2013/12/040.
67. Teppa Pannia, F.A.; García, F.; Perez Bergliaffa, S.E.; Orellana, M.; Romero, G.E. Structure of Compact Stars in R-squared Palatini Gravity. *General Relativity and Gravitation* **2017**, *49*, 25. doi:10.1007/s10714-016-2182-7.

68. Lobato, R.; Lourenço, O.; Moraes, P.H.R.S.; Lenzi, C.H.; de Avellar, M.; de Paula, W.; Dutra, M.; Malheiro, M. Neutron Stars in $f(R,T)$ Gravity Using Realistic Equations of State in the Light of Massive Pulsars and GW170817. *Journal of Cosmology and Astroparticle Physics* **2020**, *2020*, 039. doi:10.1088/1475-7516/2020/12/039.
69. Haensel, P.; Potekhin, A.Y. Analytical Representations of Unified Equations of State of Neutron-Star Matter. *Astronomy & Astrophysics* **2004**, *428*, 191–197. doi:10.1051/0004-6361:20041722.
70. Kroese, D.P.; Taimre, T.; Botev, Z.I. *Handbook of Monte Carlo Methods*; Wiley series in probability and statistics, Wiley, 2011.
71. Gill, J. *Bayesian Methods: A Social and Behavioral Sciences Approach, Third Edition*; Chapman & Hall/CRC Statistics in the Social and Behavioral Sciences, CR Press, 2014.
72. Betancourt, M. A Conceptual Introduction to Hamiltonian Monte Carlo. *arXiv:1701.02434* **2017**.
73. LIGO Scientific Collaboration and Virgo Collaboration.; Abbott. Properties of the Binary Neutron Star Merger GW170817. *Physical Review X* **2019**, *9*, 011001, [1805.11579]. doi:10.1103/physrevx.9.011001.
74. Most, E.R.; Weih, L.R.; Rezzolla, L.; Schaffner-Bielich, J. New Constraints on Radii and Tidal Deformabilities of Neutron Stars from GW170817. *Physical Review Letters* **2018**, *120*. doi:10.1103/physrevlett.120.261103.
75. The LIGO Scientific Collaboration and the Virgo Collaboration.; Abbott, R.; Abbott. GW190814: Gravitational Waves from the Coalescence of a 23 Solar Mass Black Hole with a 2.6 Solar Mass Compact Object. *The Astrophysical Journal* **2020**, *896*, L44. doi:10.3847/2041-8213/ab960f.
76. Cromartie, H.T.; Fonseca, E.; Ransom, S.M.; Demorest, P.B.; Arzoumanian, Z.; Blumer, H.; Brook, P.R.; DeCesar, M.E.; Dolch, T.; Ellis, J.A.; Ferdman, R.D.; Ferrara, E.C.; Garver-Daniels, N.; Gentile, P.A.; Jones, M.L.; Lam, M.T.; Lorimer, D.R.; Lynch, R.S.; McLaughlin, M.A.; Ng, C.; Nice, D.J.; Pennucci, T.T.; Spiewak, R.; Stairs, I.H.; Stovall, K.; Swiggum, J.K.; Zhu, W.W. Relativistic Shapiro Delay Measurements of an Extremely Massive Millisecond Pulsar. *Nature Astronomy* **2020**, *4*, 72–76. doi:10.1038/s41550-019-0880-2.
77. Linares, M.; Shahbaz, T.; Casares, J. Peering into the Dark Side: Magnesium Lines Establish a Massive Neutron Star in PSR J2215+5135. *The Astrophysical Journal* **2018**, *859*, 54. doi:10.3847/1538-4357/aabde6.
78. Demorest, P.B.; Pennucci, T.; Ransom, S.M.; Roberts, M.S.E.; Hessels, J.W.T. A Two-Solar-Mass Neutron Star Measured Using Shapiro Delay. *Nature* **2010**, *467*, 1081–1083. doi:10.1038/nature09466.
79. Antoniadis, J.; Freire, P.C.C.; Wex, N.; Tauris, T.M.; Lynch, R.S.; van Kerkwijk, M.H.; Kramer, M.; Bassa, C.; Dhillon, V.S.; Driebe, T.; Hessels, J.W.T.; Kaspi, V.M.; Kondratiev, V.I.; Langer, N.; Marsh, T.R.; McLaughlin, M.A.; Pennucci, T.T.; Ransom, S.M.; Stairs, I.H.; van Leeuwen, J.; Verbiest, J.P.W.; Whelan, D.G. A Massive Pulsar in a Compact Relativistic Binary. *Science* **2013**, *340*, 1233232. doi:10.1126/science.1233232.
80. LIGO Scientific Collaboration. LIGO Algorithm Library - LALSuite. free software (GPL), 2018. doi:10.7935/GT1W-FZ16.
81. Bingham, E.; Chen, J.P.; Jankowiak, M.; Obermeyer, F.; Pradhan, N.; Karaletsos, T.; Singh, R.; Szerlip, P.A.; Horsfall, P.; Goodman, N.D. Pyro: Deep Universal Probabilistic Programming. *J. Mach. Learn. Res.* **2019**, *20*, 28:1–28:6.
82. Hoffman, M.D.; Gelman, A.; others. The No-U-Turn sampler: adaptively setting path lengths in Hamiltonian Monte Carlo. *J. Mach. Learn. Res.* **2014**, *15*, 1593–1623.
83. Steiner, A.W.; Lattimer, J.M.; Brown, E.F. Neutron Star Radii, Universal Relations, and the Role of Prior Distributions. *The European Physical Journal A* **2016**, *52*. doi:10.1140/epja/i2016-16018-1.
84. Raaijmakers, G.; Riley, T.E.; Watts, A.L. A Pitfall of Piecewise-Polytropic Equation of State Inference. *Monthly Notices of the Royal Astronomical Society* **2018**, *478*, 2177–2192. doi:10.1093/mnras/sty1052.
85. Endrizzi, A.; Ciolfi, R.; Giacomazzo, B.; Kastaun, W.; Kawamura, T. General Relativistic Magnetohydrodynamic Simulations of Binary Neutron Star Mergers with the APR4 Equation of State. *Classical and Quantum Gravity* **2016**, *33*, 164001. doi:10.1088/0264-9381/33/16/164001.
86. Maione, F.; Pietri, R.D.; Feo, A.; Löffler, F. Binary Neutron Star Merger Simulations with Different Initial Orbital Frequency and Equation of State. *Classical and Quantum Gravity* **2016**, *33*, 175009. doi:10.1088/0264-9381/33/17/175009.
87. Anderson, D.; Yunes, N. Scalar Charges and Scaling Relations in Massless Scalar–Tensor Theories. *Classical and Quantum Gravity* **2019**, *36*, 165003. doi:10.1088/1361-6382/ab2eda.
88. Odintsov, S.D.; Oikonomou, V.K. Neutron Stars in Scalar-tensor Gravity with Higgs Scalar Potential. *arXiv e-prints* **2021**, [2104.01982].
89. Odintsov, S.D.; Oikonomou, V.K. Neutron Stars Phenomenology with Scalar–Tensor Inflationary Attractors. *Physics of the Dark Universe* **2021**, *32*, 100805. doi:10.1016/j.dark.2021.100805.
90. Raaijmakers, G.; Riley, T.E.; Watts, A.L.; Greif, S.K.; Morsink, S.M.; Hebeler, K.; Schwenk, A.; Hinderer, T.; Nissanke, S.; Guillot, S.; Arzoumanian, Z.; Bogdanov, S.; Chakrabarty, D.; Gendreau, K.C.; Ho, W.C.G.; Lattimer, J.M.; Ludlam, R.M.; Wolff, M.T. A NICER View of PSR J0030$\mathplus$0451: Implications for the Dense Matter Equation of State. *The Astrophysical Journal* **2019**, *887*, L22. doi:10.3847/2041-8213/ab451a.
91. Miller, M.C.; Chirenti, C.; Lamb, F.K. Constraining the Equation of State of High-density Cold Matter Using Nuclear and Astronomical Measurements. *The Astrophysical Journal* **2019**, *888*, 12. doi:10.3847/1538-4357/ab4ef9.
92. Raaijmakers, G.; Greif, S.K.; Hebeler, K.; Hinderer, T.; Nissanke, S.; Schwenk, A.; Riley, T.E.; Watts, A.L.; Lattimer, J.M.; Ho, W.C.G. Constraints on the Dense Matter Equation of State and Neutron Star Properties from NICER's Mass–Radius Estimate of PSR J0740$\mathplus$6620 and Multimessenger Observations. *The Astrophysical Journal Letters* **2021**, *918*, L29. doi:10.3847/2041-8213/ac089a.

 doi:10.20944/preprints202205.0073.v1

93. Lobato, R.V.; Chimanski, E.V.; Bertulani, C.A. Unsupervised Machine Learning Correlations in EoS of Neutron Stars. *arXiv e-prints* **2022**, [2202.13940]. doi:10.48550/arXiv.2202.13940.
94. Lobato, R.V.; Chimanski, E.V.; Bertulani, C.A. Cluster Structures with Machine Learning Support in Neutron Star M-R Relations. *arXiv e-prints* **2022**, [2204.01183]. doi:10.48550/arXiv.2204.01183.